MNRAS 000, 1–6 (2022) Preprint 12 May 2022 Compiled using MNRAS LATEX style file v3.0

Forced Simple Pendulum

Laura Bárbara,[1] ⋆
[1] University of Southampton, University Road, Southampton, SO17 1BJ, UK

16 May 2022

ABSTRACT

In this paper, the Runge-Kutta method was implemented in Python to solve the equation of motion of the forced simple pendulum in order to investigate ranges of driving force amplitude values for which different types of behaviour occurred. Initial rest conditions as well as a fixed damping coefficient and driving frequency were assumed. Five different kinds of motion were observed for different parameter ranges: linear periodic motion, non-linear periodic motion, rolling motion, period doubling and chaotic motion.

Key words: non-linear system – driving force – periodic motion – period doubling – chaos – runge-kutta method

1 INTRODUCTION

The pendulum has historically been one of the most investigated mechanical systems, peaking the interest of Italian physicist Galileo Galilei for the first time in the late 16th century. Years later, Galileo would postulate and eventually prove four properties of the pendulum's motion, one of which was the relation between its period and its length under small oscillation conditions, $T \propto (L/g)^{1/2}$ Matthews (2000). In the 21st century, the pendulum has made its way into virtually all classical mechanics or equivalent courses for undergraduates around the world, oftentimes as an example of Simple Harmonic Motion (SHM).

The particular physical system of interest in this work is the Forced Simple Pendulum (FSP), sometimes referred to as the harmonically-driven, linearly-damped simple pendulum. By relaxing the small angle approximation that is characteristic in the study of a pendulum's SHM, the FSP becomes a non-linear system.

Non-linearity in a dynamical system implies that it possesses two seemingly paradoxical properties, determinism and unpredictability. This behaviour is commonly referred to as 'chaos', and it can be observed in many natural and artificial systems alike, from meteorology and population evolution Letellier (2011) to stock markets Sahni (2018) and road traffic Adewumi et al. (2016). A deterministic system is that whose behaviour evolves in a unique way that is completely determined by its initial conditions. The chaos of non-linear systems comes from the fact that small differences in initial conditions will lead to wildly different solutions. Physical measurement errors or computational truncation errors, which typically grow linearly in time, now grow exponentially, effectively rendering long-term predictions of a system's behaviour impossible.

The equation of motion of the FSP is given by Equation 1 for a pendulum of mass m and length L at a given displacement θ from the vertical rest position. Besides the expected gravitational acceleration g, the pendulum experiences a damping to its motion proportional to a constant k_D and its angular velocity, as well as an external periodic driving force of magnitude F_F and frequency Ω_F

$$mL^2\ddot{\theta} + k_D\dot{\theta} + mgL\sin\theta = F_F L\cos(\Omega_F t) \tag{1}$$

The non-linear nature of the FSP is evidenced by the extreme dependence of its behaviour on the elected initial parameters, with the very delicate transitions between non-chaotic and chaotic states. The analysis of the motion of the FSP for different parameter ranges is therefore a remarkable way to gain a better understanding of the meaning of 'non-linearity' or 'chaos' in dynamical systems.

A comprehensive study of all of the different parameter ranges for which the pendulum would exhibit distinct types of behaviour would be very laborious and difficult to convey in a single piece of work. For that reason, this paper chooses to focus on the breakdown of simple periodic motion as the magnitude of the driving force is increased.

2 METHODOLOGY

The time evolution of the pendulum's position and velocity for given initial parameters can be retrieved by solving Equation 1 using the Runge-Kutta method as outlined in appendix A. This method requires the equation of motion to be written as two dimensionless coupled ordinary differential equations (ODEs), as per subsection 2.1, which will be solved simultaneously.

2.1 Dimensionless equation of motion

The first step in nondimensionalising Equation 1 is to define time in terms of the natural period of the simple pendulum at small amplitudes by introducing a dimensionless parameter τ:

$$\boxed{\tau = t\sqrt{\frac{g}{L}}}$$

The derivatives in Equation 1 may then be rewritten in terms of τ by the chain rule, as well as the cosine in the driving force term.

⋆ E-mail: ldpb1g19@soton.ac.uk

$$\frac{d^2\theta}{dt^2} = \frac{g}{L}\frac{d^2\theta}{d\tau^2}, \quad \frac{d\theta}{dt} = \sqrt{\frac{g}{L}}\frac{d\theta}{d\tau}, \quad \cos(\Omega_F t) = \cos\left(\Omega_F \tau\sqrt{\frac{L}{g}}\right)$$

And so the equation of motion becomes:

$$\frac{d^2\theta}{d\tau^2} + \frac{k_D}{mL\sqrt{gL}}\frac{d\theta}{d\tau} + mgL\sin\theta = \frac{F_F}{mg}\cos\left(\Omega_F\tau\sqrt{\frac{L}{g}}\right) \tag{2}$$

Defining three new dimensionless parameters:

$$\boxed{\eta = 1 - \Omega\sqrt{\frac{L}{g}}} \qquad \boxed{k = \frac{k_D}{mL\sqrt{gL}}} \qquad \boxed{F = \frac{F_F}{mg}}$$

The equation of motion as given in Equation 3 is now written completely in terms of dimensionless constants.

$$\frac{d^2\theta}{d\tau^2} = -k\frac{d\theta}{d\tau} - sin\theta + F\cos[(1-\eta)\tau] \tag{3}$$

As previously mentioned, in order for the Runge-Kutta method to solve a second order differential equation of motion, the equation must be separated into two coupled first order differential equations. By defining the angular velocity ω of the pendulum, Equation 3 may be given by a system of two ODEs:

$$\boxed{\frac{d\theta}{d\tau} = \omega} \qquad \boxed{\frac{d\omega}{d\tau} = -k\omega - sin\theta + F\cos[(1-\eta)\tau]} \tag{4}$$

2.2 Initial conditions and parameter values

For simplicity, and in order to focus the investigation solely on the effects of the external driving force and the damping, the pendulum was considered to begin at rest in each calculation. In other words, the angular velocity was always zero at $\tau = 0$. The initial displacement was zero for most of the calculations, only taking on different values in order to showcase properties such as period doubling and chaotic behaviour.

The parameter η was taken to be $1/3$, which means that the driving frequency is $2/3$ of the natural frequency of the pendulum. This avoids very large oscillation amplitudes of the system due to resonance while still having a short period for the driving force. Similarly, the dimensionless damping coefficient was chosen to be $k = 0.5$ to prevent very large amplitudes.

The remaining parameter F was varied, taking values from 0.2 to 1.2. The specific value chosen in each case in section 3 is explicitly stated.

2.3 Numerical analysis

The Runge-Kutta method was used to compute solutions to the ODEs in Equation 4, using the numerical integration Python function `scipy.integrate.solve_ivp` (see appendix A1). The initial values and parameters in subsection 2.2 were passed to the function, along with the ODEs, and the integration was carried out for values of τ between 0 and 300 with 100000 steps. This translates to a step length of $h = 0.003$, corresponding to a total accumulated error of the order of 10^{-10} which can be neglected.

Figure 1. Phase space diagram of the periodic motion of the FSP with initial conditions $\theta(0) = 0$, $\omega(0) = 0$, and parameters $k = 0.5$, $\eta = 1.3$ and $F = 0.2$ (blue) or $F = 0.9$ (red), for $0 < \tau < 300$. The transient behaviour was removed for readability by beginning the plot at $\tau = 50$.

3 RESULTS

3.1 Periodic motion

The phase space diagram of the FSP with parameters $k = 0.5$, $\eta = 1.3$, and starting its motion at rest and with no angular displacement, is shown in Figure 1 for F values of 0.2 and 0.9. For low values of F and once the transient motion has damped away, the oscillation amplitudes are small enough that the pendulum's phase space diagram shows an elliptical shape characteristic of a harmonically-driven, linearly-damped linear oscillator (blue line). Varying F manually, this linear behaviour was estimated to persist until $F \sim 0.7$. After this value, the amplitude of the oscillations does not satisfy the small angle approximation and the pendulum's non-linearity distorts the phase space plot (red line).

The pendulum maintains the same non-linear periodic motion, for the initial conditions and parameters given above, with increasingly larger transients until $F = 1.038$. For higher values, the driving force has large enough amplitude to rotate the transient solution away from the starting condition $\theta(0) = 0$, causing the centre of the periodic portion of the phase space diagram to be shifted by as many rotations as the transient underwent. This behaviour is shown in Figure 2, in which a driving force $F = 1.045$ rotated the transient solution once before the pendulum settled on a non-linear periodic motion.

For values of F between 1.29 and 1.39, the pendulum was found to undergo continuous rolling motion, which is comprised of multiple subsequent full turns over itself in the same direction, as illustrated in Figure 3 for $F = 1.34$. While both the angular velocity and the oscillation amplitude of the pendulum behave in a periodic fashion, the latter undergoes continuous revolutions.

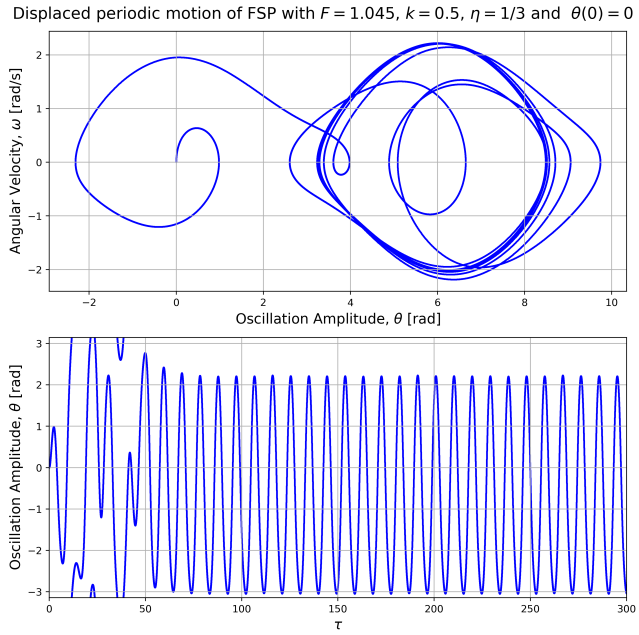

Figure 2. Phase space diagram (top) and angular displacement-time graph (bottom) of the periodic motion of the FSP with initial conditions $\theta(0) = 0$, $\omega(0) = 0$, and parameters $F = 1.045$, $k = 0.5$ and $\eta = 1.3$, for $0 < \tau < 300$.

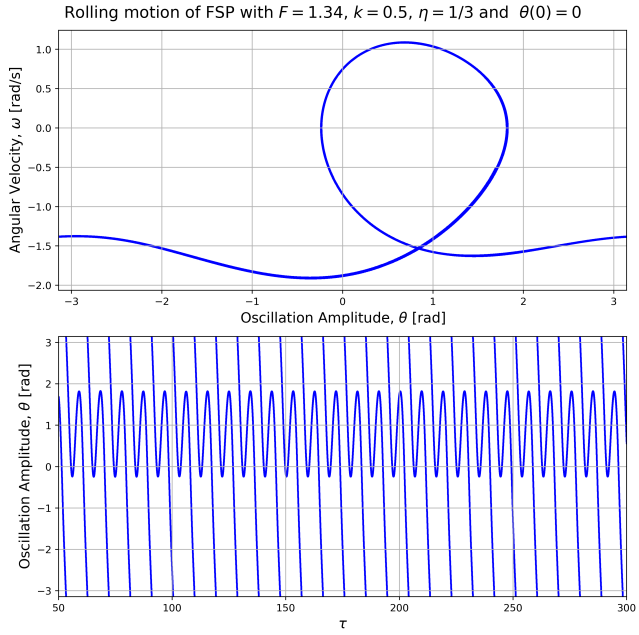

Figure 3. Phase space diagram (top) and angular displacement-time graph (bottom) of the rolling motion of the FSP with initial conditions $\theta(0) = 0$, $\omega(0) = 0$, and parameters $F = 1.34$, $k = 0.5$ and $\eta = 1.3$, for $0 < \tau < 300$. The transient behaviour was removed for readability by beginning the plot at $\tau = 50$.

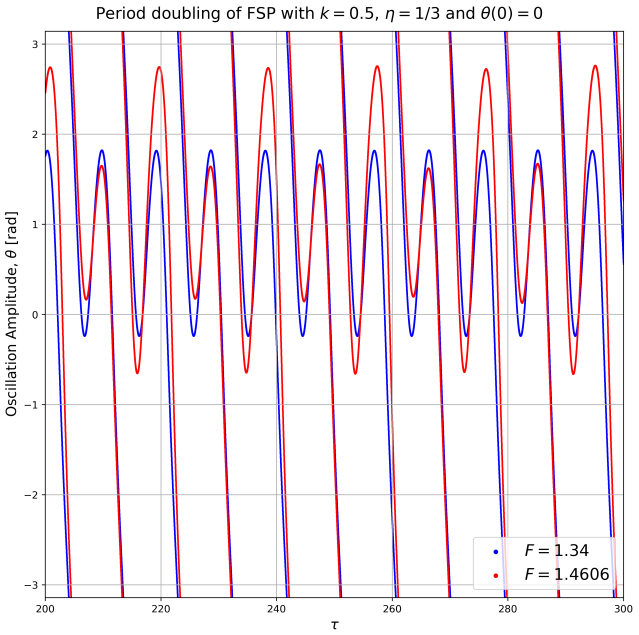

Figure 4. Angular displacement-time graph of period doubling phenomenon of the FSP with initial conditions $\theta(0) = 0$, $\omega(0) = 0$, and parameters $k = 0.5$, $\eta = 1.3$ and $F = 1.34$ (blue, period-one) or $F = 1.4606$ (red, period-two), for $0 < \tau < 300$. The transient behaviour was removed and the interval of time shown was shortened for readability by beginning the plot at $\tau = 200$.

3.2 Transition to chaos

For very specific values of F, a particularly interesting phenomenon called 'period doubling' occurs. In Figure 4 the variation of θ with τ was plotted for both the rolling motion case outlined in subsection 3.1 ($F = 1.34$) in blue and $F = 1.4606$ in red. The plot shows that for $F = 14606$ the system exhibits periodic rolling motion with double the period as for $F = 1.34$. This behaviour introduces another characteristic of nonlinear systems: their response to a single driving frequency may contain, not only the frequency itself, but also its harmonics and, for the case of period doubling, subharmonics Giordano & Nakanishi (2005). At higher values of F, the period doubling would continue in binary multiples, which would ultimately result in chaos.

The expected chaotic behaviour occurs when $F > 1.8$, after which the phase space diagrams of the pendulum are highly sensitive to changes in the initial conditions of the system. Figure 5 clearly showcases this, where starting the pendulum at $\theta(0) = -0.15$ (blue), $\theta = 0$ (red) and $\theta = 0.15$ (green) yields distinct phase space diagrams. One interesting feature that all three diagrams have in common is that, within the chaotic behaviour, some structure can still be retrieved, such as occasional nearly closed orbits.

4 CONCLUSIONS

This paper aimed to investigate the non-linearity of the forced simple pendulum as a dynamical system, making use of the Runge-Kutta method in integrating its equation of motion in order to qualitatively analyse the behaviour exhibited for a number of different driving force amplitudes. The results obtained from the Runge-Kutta method using

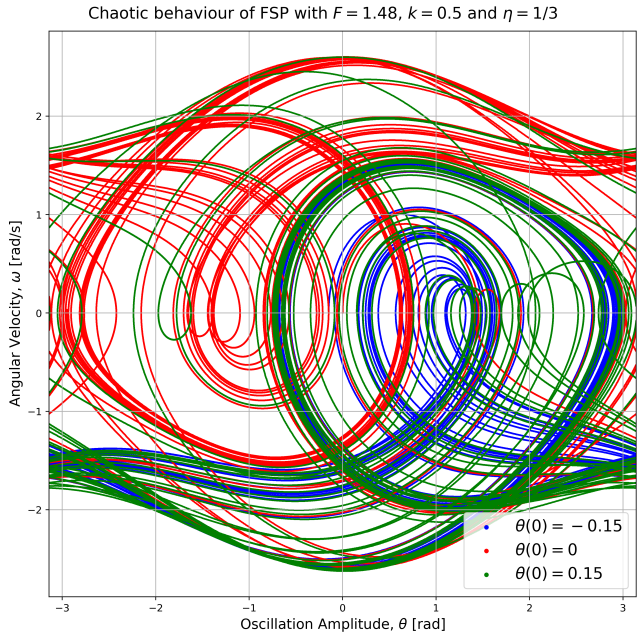

Figure 5. Phase space diagram of the chaotic motion of the FSP with initial conditions $\theta(0) = [-0.15, 0, 0.15]$, $\omega(0) = 0$, and parameters $F = 1.2$, $k = 0.5$ and $\eta = 1.8$, for $0 < \tau < 300$.

a step-size of 0.003 had a negligible total accumulated error of the order of 10^{-10}.

Assuming initial rest conditions and keeping the damping and driving frequency dimensionless parameters constant at $k = 0.5$ and $\eta = 1/3$, respectively, the FSP underwent various distinct regimes of motion as the magnitude of the driving force was increased manually. It was found that for values of $F < 0.7$, the pendulum actually maintained a linear periodic motion due to the external force being damped enough for the oscillation amplitudes to remain within the range of the small amplitude approximation. Between 0.7 and 1.038 the pendulum still oscillated periodically, though with amplitudes which were no longer damped enough to agree with the linear model, thus showing the first signs of its non-linearity through the distortion of the phase-space diagrams. When F takes values between 1.29 and 1.39, the system underwent rolling motion, meaning the pendulum carried out periodical subsequent complete oscillations 'looping over itself'. Furthermore, the 'frequency mixing' which is characteristic of non-linear systems was observed at $F = 1.4606$, for which the period of the oscillations doubled. Finally, for values of $F > 1.8$ the system's motion became chaotic.

REFERENCES

Adewumi A., Kagamba J., Alochukwu A., 2016, Mathematical Problems in Engineering, 2016, 1

Baba I. A., Yusuf A., Nisar K. S., Abdel-Aty A.-H., Nofal T. A., 2021, Results in Physics, 20, 103716

Butcher J. C., 1963, Journal of the Australian Mathematical Society, p. 185–201

Dormand J., Prince P., 1980, Journal of Computational and Applied Mathematics, 6, 19

Fadlisyah M., 2014, PhD thesis, Faculty of Mathematics and Natural Sciences, University of Oslo

Giordano N. J., Nakanishi H., 2005, Computational Physics, 2 edn. Pearson, Upper Saddle River, NJ

Hong J., Li C., 2006, Journal of Computational Physics, 211, 448

Huang S. J., Yu J., 2004, SSRN Electronic Journal

Khan M., Shah S. W., Ullah S., Gómez-Aguilar J., 2019, Nonlinear Analysis: Real World Applications, 50, 144

Letellier C., 2011, Chaos in Nature. WORLD SCIENTIFIC, doi:10.1142/8312

Maleki H., Safaei M. R., Alrashed A. A. A. A., Kasaeian A., 2018, Journal of Thermal Analysis and Calorimetry, 135, 1655

Matthews M. R., 2000, in , Time for Science Education. Springer Netherlands, pp 95–120, doi:10.1007/978-94-011-3994-6_5

Pujotomo I., Iwa G., Ridwan G., Uno B. S., 2016, in 2016 International Seminar on Intelligent Technology and Its Applications (ISITIA). IEEE, doi:10.1109/isitia.2016.7828702

Sahni R., 2018, in 2018 9th International Conference on Computing, Communication and Networking Technologies (ICCCNT). IEEE, doi:10.1109/icccnt.2018.8494103

Simangunsong L., Mungkasi S., 2021, in INTERNATIONAL CONFERENCE ON LIFE SCIENCES AND TECHNOLOGY (ICoLiST 2020). AIP Publishing, doi:10.1063/5.0052550

Sterner E., 1997, BIT Numerical Mathematics, 37, 164

Suli E., Mayers D. F., 2003, An Introduction to Numerical Analysis. Cambridge University Press, Cambridge, England

APPENDIX A: RUNGE-KUTTA METHOD

The Runge-Kutta methods are a family of explicit and implicit methods of numerical analysis used to solve initial value problems. These methods can provide approximate solutions of ODEs which have well defined initial boundary conditions.

Let some first order differential equation with initial condition $y(t_n) = y_n$ be defined as:

$$\frac{dy}{dt} = f(t, y) \tag{A1}$$

An approximation for $y(t)$ can then be found using a given explicit Runge-Kutta method, defined in Equation A2

$$y_{n+1} = y_n + h \sum_{i=1}^{s} b_i k_i, \tag{A2}$$

Where h is the step size between t_n and t_{n+1}, and k_i is given by:

$$\begin{aligned}
k_1 &= f(t_n, y_n),\\
k_2 &= f(t_n + c_2 h, y_n + h(a_{21} k_1)),\\
k_3 &= f(t_n + c_3 h, y_n + h(a_{31} k_1 + a_{32} k_2)),\\
&\vdots\\
k_s &= f(t_n + c_s h, y_n + h(a_{s1} k_1 + a_{s2} k_2 + \cdots + a_{s,s-1} k_{s-1})).
\end{aligned}$$

Where the integer s dictates the number of stages of the specific Runge-Kutta method. The matrix $[a_{si}]$, the weights b_i and the nodes c_s are also particular to each method, and have been defined by Butcher in Butcher (1963). For each method, the corresponding values are typically quoted in a Butcher tableau, which takes the form of the example below for an explicit method.

0					
c_2	a_{21}				
c_3	a_{31}	a_{32}			
$\vdots$	$\vdots$		$\ddots$		
c_s	a_{s1}	a_{s2}	$\cdots$	$a_{s,s-1}$	
	b_1	b_2	$\cdots$	b_{s-1}	b_s

This project made use of the fourth-order Runge-Kutta method, commonly referred to as "RK4". The RK4 method approximates the value of $y(t)$ using the weighted average of four slopes multiplied by the size of the increment h. Its Butcher tableau is given below Suli & Mayers (2003).

0				
1/2	1/2			
1/2	0	1/2		
1	0	0	1	
	1/6	1/3	1/3	1/6

A graphical representation of the RK4 method is shown in Figure A1, taken from Fadlisyah (2014). The known initial conditions t_n and y_n are used to calculate a slope k_1 at the beginning of the interval (t_n). The values of k_1 and y_n are then used to calculate a slope k_2 at the midpoint of the interval $(t_n + \frac{1}{2}h)$. This process is repeated for a third slope k_3 at the same midpoint, using the value of k_2. A final slope k_4 is then calculated with k_3 at the end of the interval $(t_n + h)$. Finally, a weighted average of the four slopes is used to obtain the approximation for y_{n+1}, with the two midpoint slopes contributing twice as much.

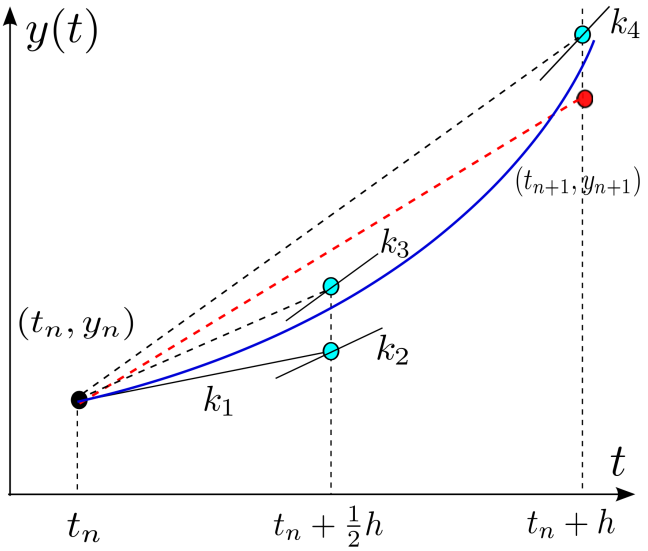

Figure A1. Graphical representation of the RK4 method, explicitly showing the slopes calculated in the interval between t_n and $t_n + h$.

As with any numerical analysis technique, the Runge-Kutta methods provide an approximate solution of the equation in study, which differs from the real solution by a certain amount. This discrepancy is known as the global truncation error (GTE), and it stems from the accumulation of the local truncation error (LTE) at every step in the computation. Since the RK4 method is a fourth-order expansion, its LTE is on the order of $O(h^5)$ while its GTE is on the order of $O(h^4)$ Suli & Mayers (2003). Thus, for small enough values of h (i.e. $h \ll 1$) the RK4 method will produce an accurate approximation of the real solution. The RK4 method offers an excellent balance between a high convergence rate and low computational intensity, which has ultimately set it apart from other Runge-Kutta methods such as the Euler method.

A1 Runge-Kutta in Python

The `scipy.integrate` sub-package offers a function which solves first-order differential equations through a number of methods. The default method used by the `solve_ivp` function is the 'RK45', an embedded Runge-Kutta method which employs both a fourth and a fifth-order method in tandem. Embedded methods introduce the ability to estimate the LTE of each step, which can be controlled by using an adaptive step-size (i.e. a smaller value of h in ranges where the solution changes rapidly). Additionally, the adaptive step-size ensures the stability of the embedded method over a larger region than its individual explicit counterparts Dormand & Prince (1980).

The `solve_ivp` function was used in this project to solve the set of coupled ODEs from section 2. The required inputs for `solve_ivp` are the right-hand side of Equation A1 as an input function, the initial state of the system, and the interval of integration. Optional ar-

guments can be included, such as an array of specific points for which to integrate the function and the preferred method of integration to use.

A2 Applications of Runge-Kutta

The outlined robustness and efficiency of the Runge-Kutta family have led to applications of these methods in a large number of fields in both academia and industry. Some of these applications are described below.

A2.1 Applications in Academia

Hong & Li (2006) built on previous work done by the authors by studying the results of multi-symplectic Runge–Kutta (MSRK) methods in solving the nonlinear Dirac equation, which extends general relativity to matter that possesses spin. The MSRK methods are stable and convergent with respect to the conservation laws of energy, momentum and charge, making them ideal for numerical analysis in quantum physics.

In Maleki et al. (2018), an embedded RK45 method is used to study the heat transfer and fluid flow of a pseudo-plastic non-Newtonian nanofluid over a permeable surface under both injection and suction conditions. The governing equations of the system are the continuity, momentum and energy PDEs, which can be converted into ODEs through similarity solutions. The RK45 method is employed to solve the obtained ODEs.

Sterner (1997) used a blend of explicit and semi-implicit Runge-Kutta methods to solve the compressible Navier-Stokes equations in two dimensions, neglecting body force and heat flux. This new method combines a two-stage explicit method with a two-stage semi-implicit method, which consists of explicit time integration in the stream-wise direction and implicit integration in the body-normal direction. The blended method was proven to be efficient for high Reynolds number (i.e. turbulent) flows.

A2.2 Applications in Industry

Implicit Runge-Kutta methods can be used in finance in the analysis of continuous-time affine asset pricing models such as zero-coupon bond pricing Huang & Yu (2004), which typically involve finding the solution to a partial differential equation (PDE). Many affine asset prices have closed or nearly-closed form expressions, meaning the PDE can be decomposed into a system of ODEs which is solved numerically. Commonly, these ODEs will involve stiffness, which creates a number of practical difficulties for explicit Runge-Kutta methods due to their finite region of absolute stability.

In epidemiology, compartmental models are widely used in the mathematical modelling of the spread and recovery rate of infectious disease by characterising the rate of change in the proportion of people in each compartment through ODEs. These models naturally lend themselves to Runge-Kutta methods as the numerical analysis technique of choice to solve those ODEs. Some of the more prominent diseases in recent years have been modelled through Runge-Kutta methods, such as HIV Simangunsong & Mungkasi (2021), the Zika virus Khan et al. (2019), and COVID-19 Baba et al. (2021).

The stability of electric power systems can also be analysed and improved using Runge-Kutta methods. Pujotomo et al. (2016) employed second and fourth-order Runge-Kutta methods to solve the swing equation, which characterises the transient stability of a power system through the load angle. The Runge-Kutta methods minimised the values of the load angle and, thus, loss of synchronism, maintaining transient stability.

This paper has been typeset from a TEX/LATEX file prepared by the author.